Proceedings of the Seventh International Conference on
Railway Technology: Research, Development and Maintenance
Edited by: J. Pombo
Civil-Comp Conferences, Volume 15, Paper 3.1
Civil-Comp Press, Edinburgh, United Kingdom, 2026
ISSN: 2753-3239, doi: 10.4203/ccc.15.3.1

Design of a Wheel-Rail Test Rig: A Case Study on Fatigue Assessment of the Frame

S. Suutarinen[1], P. Salmenperä[2], H. Luomala[3] and X. Yu[1]

[1] Machine Dynamics Group, Faculty of Engineering and Natural Sciences, Tampere University, Finland
[2] VR Fleetcare, VR Group, Finland
[3] Research Centre Terra, Tampere University, Finland

Abstract

Experimental wheel–rail contact analysis is essential for rail vehicle stability, safety, ride comfort, and component life cycle. Compared with field tests, laboratory testing provides a controlled and systematic environment for conducting a wide range of experiments. At Tampere University, a full-scale wheel–rail test rig has been designed and built to investigate wheel–rail interaction, including contact location, contact forces, contact patch characteristics, wheel–rail wear, rolling contact fatigue, and the performance of adhesion and friction modifiers. The rig consists of a structural frame, a full-sized wheel, and a carriage for mounting the rail. Given the high load levels and the large number of accumulated load cycles, the structural fatigue of the test rig itself must be carefully assessed. In particular, joints and welded regions subjected to highly concentrated stresses require enhanced design to ensure safe operation and extend the service life of the machine. This work presents a case study on the fatigue assessment of the supporting frame of a full-scale wheel–rail test rig, aiming to support and guide future researchers in the design and evaluation of experimental facilities subjected to heavy loads and cyclic operating conditions by illustrating the necessity of fatigue assessment in the early design.

Keywords: full scale, wheel-rail interaction, structural analysis, life time estimation, finite element analysis, mechanical design.

1 Introduction

The contact mechanics between railway wheels and rails constitute a complex problem influenced by several factors, including wheel–rail geometry and wear [1], track irregularities [2], and the presence of friction modifiers at the interface [3]. Parameters contributing to wear and rolling contact fatigue are typically of primary interest in many studies [4]. Compared with field tests, laboratory experiments provide a controlled environment in which these parameters can be systematically varied. Such testing is essential for the understanding of wheel–rail interaction and for supporting the development of safer and more reliable railway systems.

Several test rig designs exist and can be broadly classified into scaled-down and full-scale configurations. These can be further categorized by test type, twin-disk rigs [5], wheel on straight track [6], wheel on curved track [7], and bogie setups [8]. The primary advantage of full-scale testing is that it eliminates the need for scaling factors, thereby providing data that more accurately represent real operating conditions. However, tests involving a full bogie are often costly. As a result, full-scale wheel-on-track test rigs offer a practical compromise, retaining realistic contact conditions.

However, full-scale testing requires the application of high loads at the wheel–rail interface, and due to the cyclic nature of the experiments, the supporting frame is susceptible to fatigue. The accumulation of load cycles can significantly affect the operational safety of the test rig, particularly in regions subjected to highly concentrated stresses, such as near hydraulic actuator attachments. Limited attention has been given in the literature to fatigue of the test rig structure itself, either during the design phase or throughout its service life.

This paper presents a case study of fatigue assessment for the supporting frame of a full-scale wheel–rail test rig that is built at Tampere University, highlighting the importance of fatigue evaluation in design phase and in defining safe operating limits. The design of the rig follows the work of [6]. The overall view of the test rig is shown in Figure 1. In this study, adjusted load level of 25t reported in the literature [3,6] and 13t typical for Finnish railways are compared as operating conditions for the rig. Although the rig has not yet been put into service and the exact loading history is therefore unknown, the simplified loading scenario provides valuable insight into the importance of accounting for fatigue during the design of wheel–rail test rig and providing information about possible critical locations. While plastic capacity under extreme loads is an important consideration for safe operation, it is not addressed in this paper. It is also noted here, that the weld fabrication quality affects the fatigue strength, but that discussion is left outside of this paper, see [9] for reference.

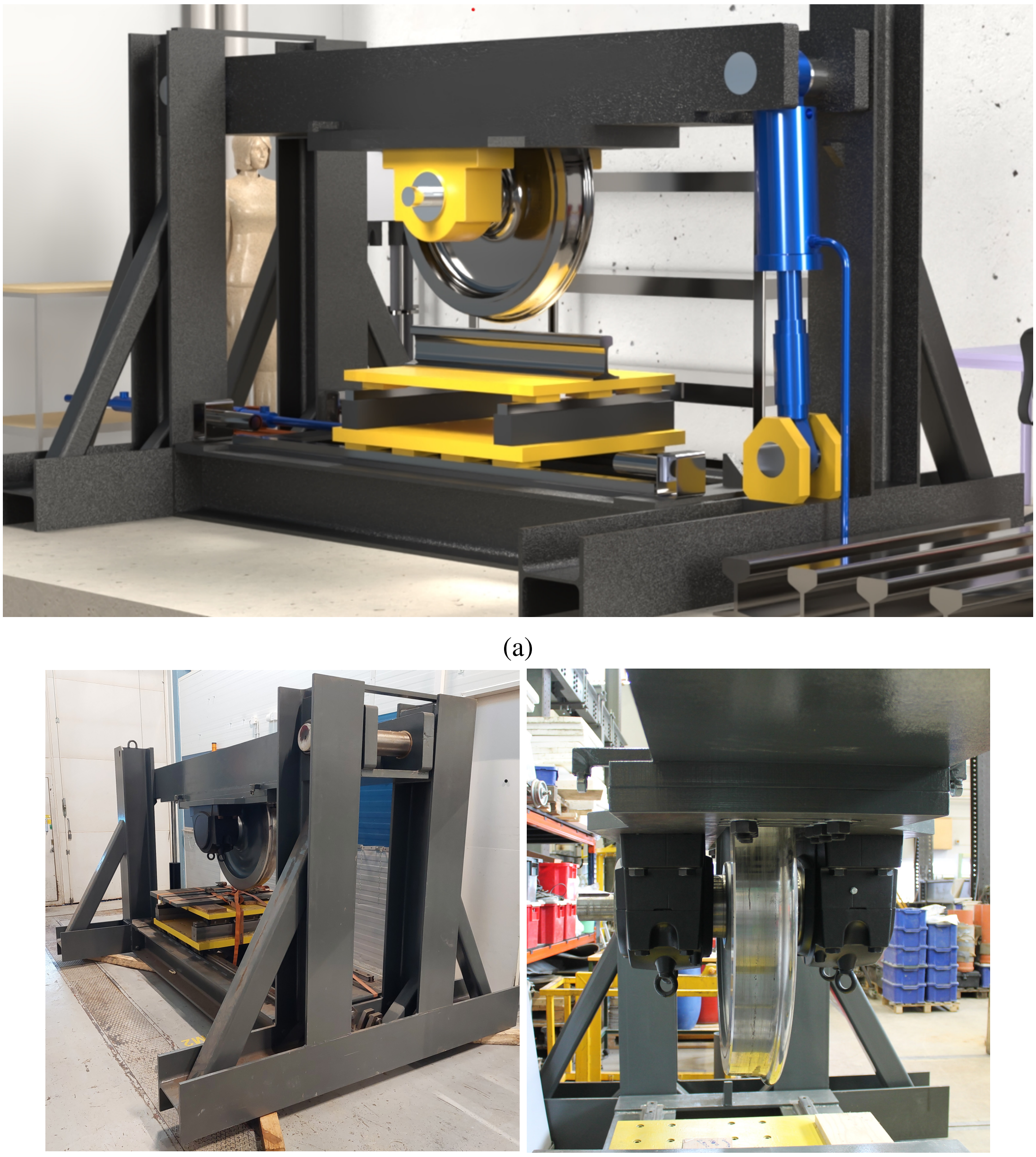

(a)

(b)

(c)

Figure 1: Overview of the full scale wheel-rail test rig at Tampere University (a) in 3D drawing and (b,c) in real life [10].

2 Description of the test rig

The test rig consists of upper and lower frames connected by vertical columns. The upper frame transfers applied loads to the columns, which transfers them to the ground through the lower frame and anchorage system. The overall dimensions of the structure are approximately 3.5 m in length, 2.5 m in width, and 2.2 m in height. The geometry and main dimensions are shown in Figure 2. The frame's material is structural steel S355. The material parameters used in the analysis are taken from [11] and shown in Table 1.

A simplified unidirectional work cycle for a wheel–rail test rig can be described as follows: (1) the wheel is pressed down, (2) the rail is moved to the opposite end, (3) the wheel is lifted and the cycle is repeated. The cycle used in this case study is based on the simplified sequence above. Two different load levels are considered, 13 t wheel load with 3.5 t longitudinal load and 25 t wheel load with 6.7 t longitudinal load. A rough estimate of the number of cycles during the test rig's service life is estimated to be 10^7.

Vertical wheel loads are applied by a hydraulic cylinder installed at one end of the frame. Longitudinal loads are generated by an second hydraulic cylinder located at the opposite end of the frame. The structure is rigidly fixed to a concrete slab at both ends, resulting in a statically indeterminate support condition. As a result, structural deformations cause load transfer between the steel frame and the concrete foundation. The hydraulic control system produces a cycle time of approximately 4–5 s (0.20–0.25 Hz). Given that the first natural frequency of the structure is approximately 8 Hz, the response can be considered quasi-static, and the structural assessment is therefore conducted without dynamic amplification factors.

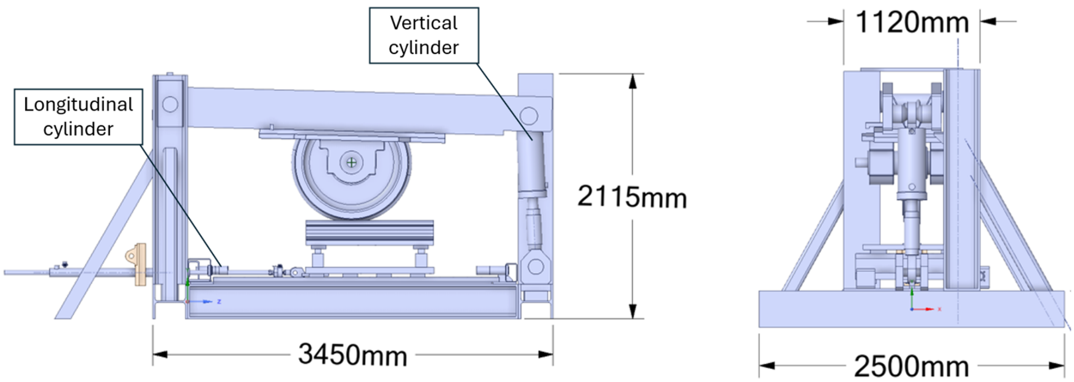

Figure 2: Test rig with overall dimensions.

Material parameter	**S355**	**Bolt 8.8**	**Bolt 10.9**	**Bolt 12.9**
Elastic modulus [GPa]	210	210	210	210
Poisson's ratio [-]	0.30	0.3	0.3	0.3
Yield strength [MPa]	355	640	900	1080
Ultimate strength [MPa]	510	800	1000	1200
Density [kg/m^3]	7850	-	-	-

Table 1: Material properties of structural steel and bolt grades used in the analysis of the test rig.

3 Design criteria

The fatigue standards typically used in engineering practice are Eurocode 3 Part 1-9 [12], and the IIW recommendations [13]. In this study, fatigue verification was performed using the nominal stress, hot-spot stress, and effective notch stress approaches. The choice of method depended on the complexity of the structural detail and was primarily based on the IIW guidelines. The nominal stress is defined as the stress in the connection without accounting for the local effects of the weld. For a simple T-joint subjected to a normal force, it is calculated as the applied force divided by the cross-sectional area. The hot-spot stress represents the structural stress at the weld toe and is obtained by linearly extrapolating stress values near the weld toe. The effective notch stress approach accounts for the nonlinear stress distribution at the weld toe by explicitly considering the weld geometry and is calculated from notch stress using predefined modeling techniques. In this paper, keyhole type of hole were modeled to the weld root with the radius $r = 1$. The different stress types are illustrated in Figure 3.

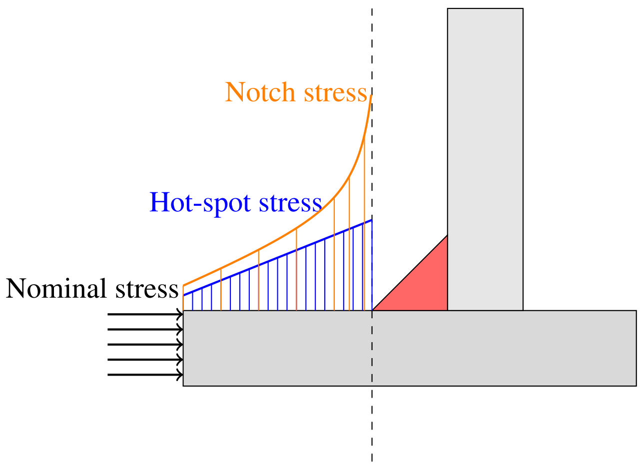

Figure 3: Different stress types, nominal, hotspot and notch stress defined in [13]

.

Fatigue resistance is typically determined from S–N curves provided in the aforementioned standards. These curves depend on the type of connection, such as butt welds or fillet welds, and are classified by a fatigue strength (FAT) class. The number associated with the FAT class represents the stress range that the detail can sustain for 2×10^6 load cycles. For example, FAT 36 indicates that the structural detail can withstand a stress range of 36 MPa for total of 2×10^6 number of cycles. The fatigue resistance at other stress levels follows a power-law relationship, where the number of cycles to failure depends on the applied stress range raised to a constant exponent. In this paper, the IIW-type S–N curve is adopted, in which the curve is divided into two regions: a slope $m_1 = 3$ for up to 1×10^7 number of cycles and slope $m_2 = 5$ for more than 1×10^7 number of cycles. The S–N curve used in the analysis is illustrated in the Figure 4 for fatigue class FAT 36.

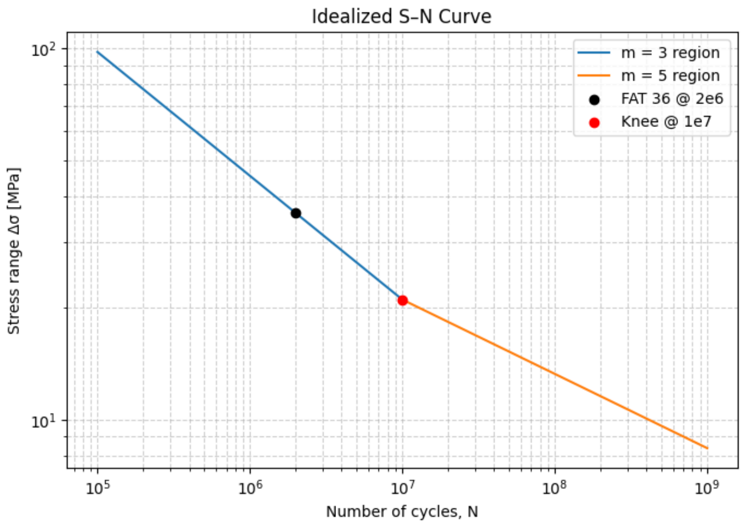

Figure 4: A SN curve shape used in the analysis. Example for FAT 36.

For simple connections, nominal stress method was used. It should be noted that extraction of nominal stresses from the FEM model requires engineering judgment: macroscopic stress raisers should be included, while local stress concentrations caused by connection details or numerical singularities should be excluded. The structure is a beam frame, so the representative nominal stress was taken as normal stress along the beam. The hotspot and effective notch stresses are more defined and can be extracted from the model using rules defined in aforementioned standards. The effective notch stress was calculated using von Mises equivalent stress, therefore FAT 200 was used instead of typical FAT255 for effective notch stress method [14].

First, the structure was screened using the maximum nominal stress ranges in each direction and critical locations - welds having high maximum ranges - were identified. The number of cycles to reach the allowable fatigue damage was then calculated for each critical location. The rainflow counting algorithm was used to extract representative stress cycles from the variable-amplitude loading. The Palmgren–Miner damage sum was then calculated from the extracted cycles, and the allowable damage for welded details was limited to 0.5 in accordance with IIW guidance [13], since in reality, the loading is variable amplitude type. A partial safety factor of 1.15 was applied, reducing the fatigue class value. This simple approach allows the identification of the most fatigue-sensitive regions of the frame, highlights potential sites for future damage initiation, and provides initial guidance on the possible range of cycles to failure for the critical details

4 FEM Analysis

The main focus in the FEM analysis was on the steel frame. therefore, the geometry was simplified and the rail and sledge was modeled only to transfer the load. The beam frame geometry was modeled as a mid-surface model and cylinders, pins and bolts were modeled as beam elements. Solid elements were used in the sub-models or locations where the geometry cannot be accurately represented by a mid-surface model. For the effective notch stress model, quadratic solid elements were used. The finite element model was created in Ansys Mechanical 2024R2 finite element software. The global finite element model alongside the mesh is shown in Figure 5.

The concrete slab was not included in the model, but foundation bolts were modeled together with the foundation plates. Fixed "dummy plates" with contact between the foundation plates were included to allow possible uplift of the frame. The bolted connections were not pretensioned and frictionless contacts were modeled between contacting surfaces. Welds were modeled using a shared mesh.The load was applied to the distributing geometries modeled with coarse mesh. Gravity was applied to all bodies as acceleration.

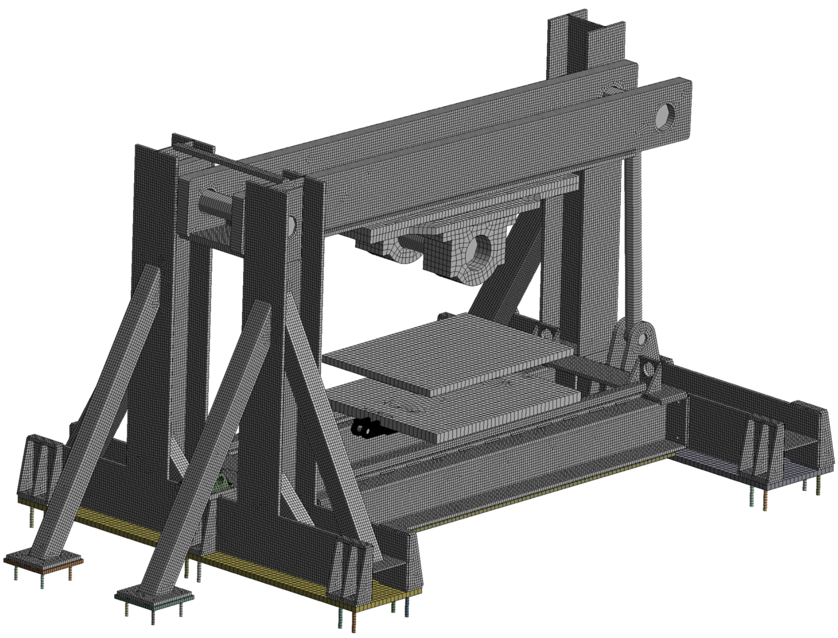

Figure 5: Overview and mesh of the global test rig FEM model.

5 FEM analysis results

Due to the large number of potential critical locations in the frame, the areas requiring more detailed fatigue assessment must first be filtered. In this simplified study, the

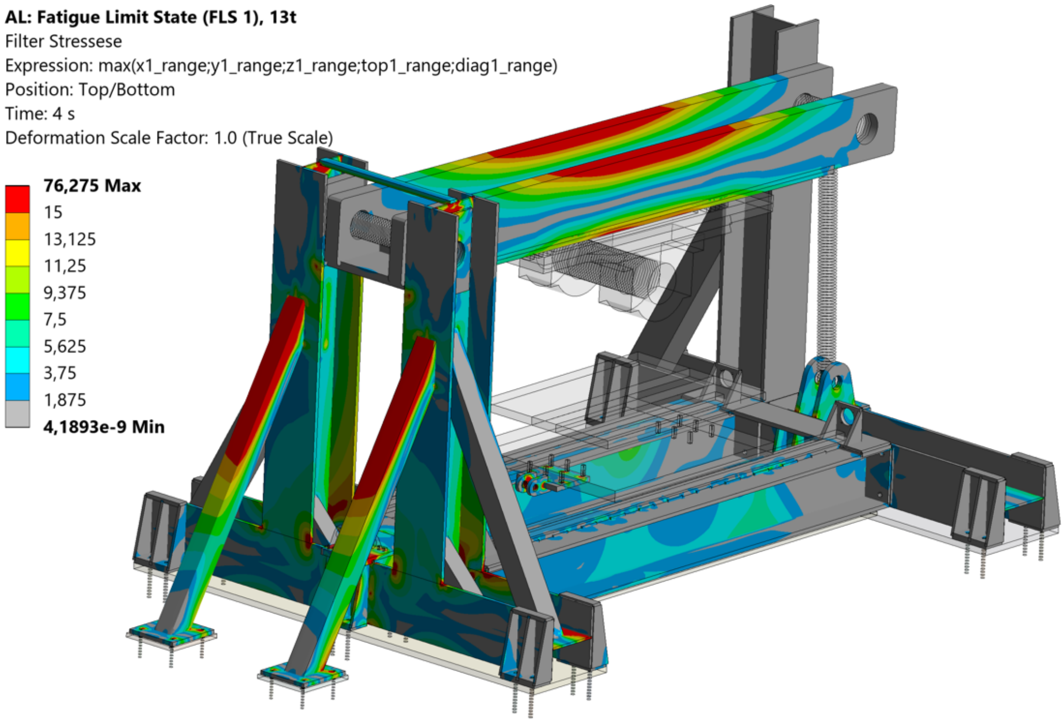

Figure 6: The overview of the maximum stress ranges calculated from different normal stress directions. In the red areas, the maximum stress range is over the filtering value 15 MPa.

filtering was performed using the lowest fatigue detail class, FAT 36, and by determining the stress range corresponding to the estimated 1×10^7 available cycles when considering the allowable damage limit. This resulted in a threshold stress range of 15 MPa. The maximum stress cycle values were calculated from the maximum and minimum stresses over time in each normal direction. These maximum cycle values are shown in Figure 6. Figure 7 highlights the locations where the maximum stress range exceeds the filtering threshold, shown in red, and marks the critical weld locations identified in this case study as detail numbers. In the Table 2 the pictures of the chosen weld details are presented alongside with description of the connection. It can be seen that most critical areas are the connections of the load carrying column, the bracing diagonals and the cylinder connections. Total of 7 details were chosen for the analysis.

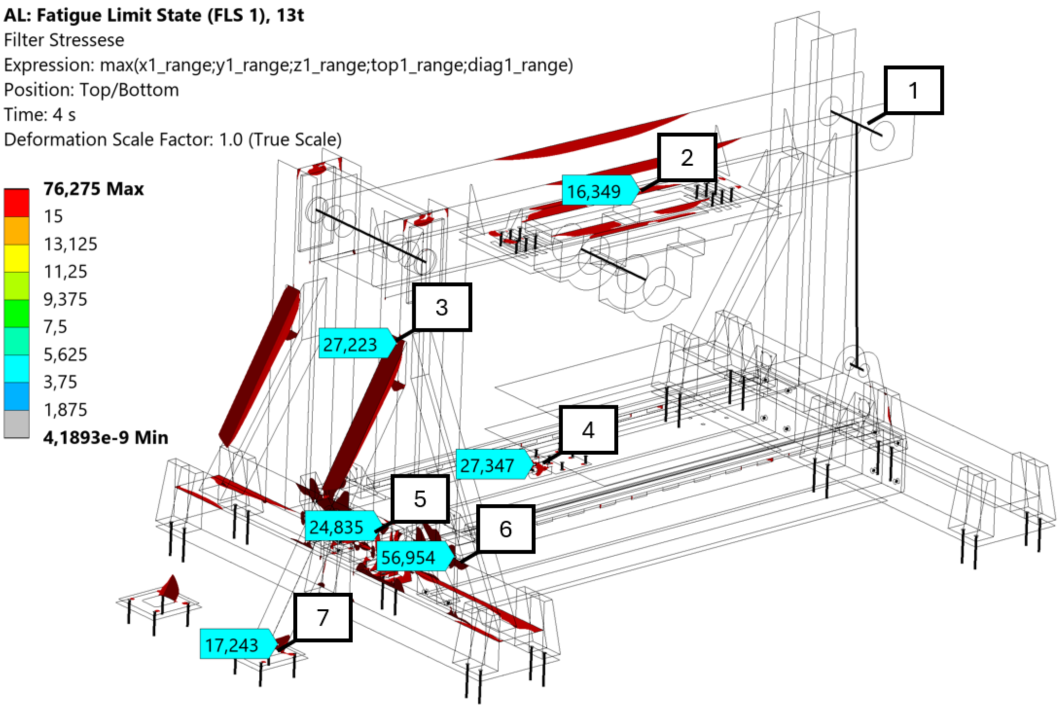

Figure 7: Chosen weld details from the areas shown in red, where maximum nominal stress range is over 15 MPa.

Details			Details		
No.	**Detail**	**Name**	**No.**	**Detail**	**Name**
1	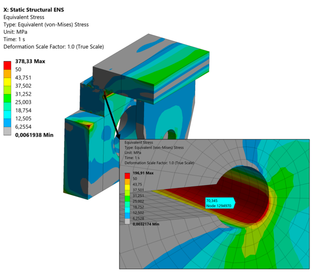	Fillet weld of the vertical cylinder connection, ENS	2	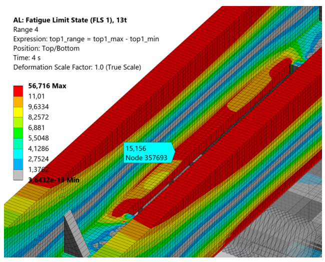	Manual longitudinal fillet weld of the top beam, Nominal stress
3	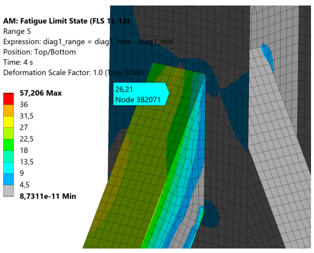	Fillet weld of the diagonal bracing, Nominal stress	4	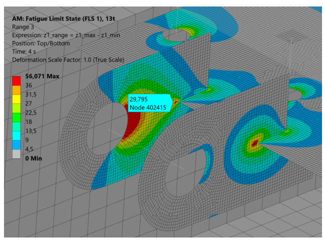	Groove weld of the longitudinal cylinder connection, Hot-spot

Continued on next page

Details			Details		
No.	**Detail**	**Name**	**No.**	**Detail**	**Name**
5	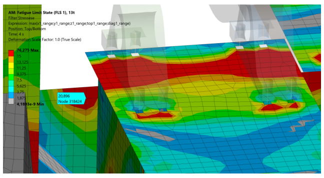	Groove weld of the cylinder support stiffener plate, Nominal stress	6	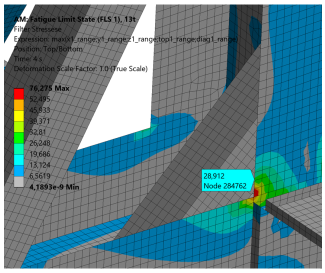	Column to base frame, intersecting flanges butt weld, Nominal stress
7	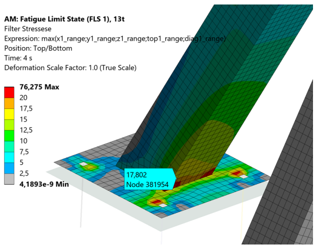	Diagonal fillet weld to base plate, Nominal stress			

Table 2: Chosen weld details, overview and description

In the Figure 8, the stresses for the 13 t load case are shown over the work cycle. Many details exhibit simple stress fluctuations, and several are located in regions where either the wheel load or the longitudinal load is the governing factor. For example, Detail 1 is primarily influenced by the vertical cylinder load during the cycle, whereas Detail 4 is governed by the longitudinal cylinder load during the sledge movement. Details 3, 5, 6, and 7 are similarly governed by the sledge movement, while Detail 2 is mainly affected by the wheel load.

For the ENS-based calculation (detail 1), fatigue class FAT 200 is used, while the hot-spot detail (detail 4) is assigned FAT 100. Potential root-side fatigue details (details 3 and 7) are evaluated using FAT 36, reflecting the possible root side failure mode. Detail 2 is a longitudinal fillet weld; therefore FAT 90 is applied. Detail 5 corresponds to a bending-dominated T-connection, and FAT 71 is assumed because weld toe failure is the governing mode [15]. For detail 6, transverse flange connections FAT 50 is used. Table 3 summarizes the results for the 13 t and 25 t wheel load cases, including the selected fatigue classes, extracted stress ranges, and calculated fatigue lives.

From the results presented in Table 3, the dramatic influence of load level on fatigue life is evident. For details operating in the m_1 slope region, the lower load level results in approximately an eight times increase in fatigue life. If the stress range of a detail lies below the knee point, the improvement would be even greater. This is illustrated, for example, by Detail 1, where the increase in load shifts the governing region from the m_2 slope to the m_1 slope.

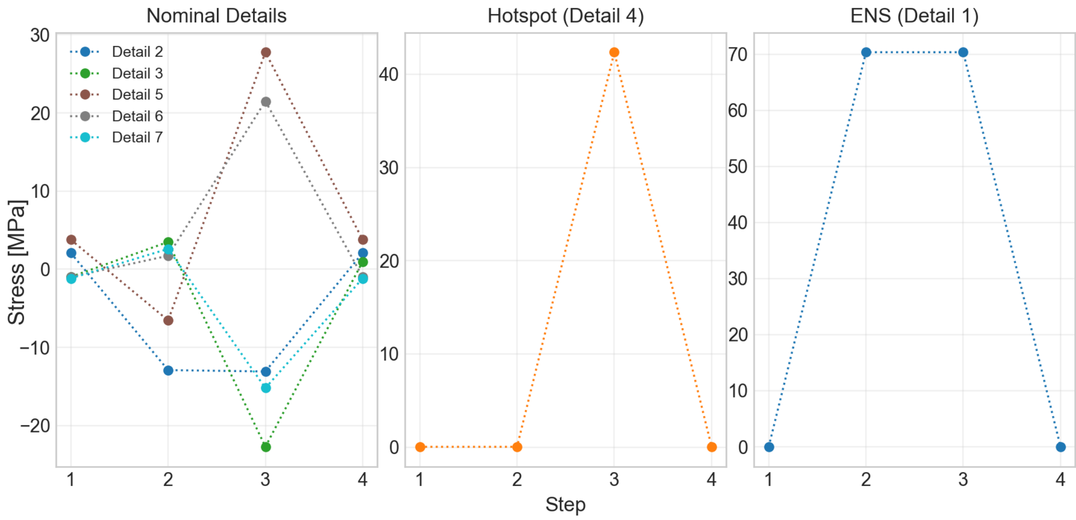

Figure 8: Stresses during work cycle, for each detail. Separated into nominal, hotspot and effective notch stresses. Wheel load 13t

Table 3: Fatigue assessment results with different wheel loading conditions

		Wheel load 13 t		**Wheel load 25 t**	
Detail No.	**Method + FAT**	**Ranges [MPa]**	**Cycles**	**Ranges [MPa]**	**Cycles**
1	ENS, FAT 200	70	3.2×10^7	133	2.2×10^6
2	Nominal stress, FAT 90	15	7.0×10^8	29	4.7×10^7
3	Nominal stress, FAT 36	26 , 3	1.8×10^6	49 , 3	2.6×10^5
4	Hot spot, FAT 100	42	1.3×10^7	81	1.2×10^6
5	Nominal stress, FAT 71	34	6.8×10^6	66	8.0×10^5
6	Nominal stress, FAT 50	22	9.3×10^6	43	1.0×10^6
7	Nominal stress, FAT 36	18	5.8×10^6	34	7.8×10^5

6 Conclusions

This paper discusses the importance of fatigue design in the development of a wheel–rail interaction test rig. The presented case study demonstrates the substantial influence of load level on the expected fatigue life of welded details. It is therefore emphasized that fatigue considerations should be incorporated as early as possible in the design process. While the choice of connection detail can improve fatigue performance through the selection of higher FAT classes, the overall stress level is primarily governed by the structural geometry.

In addition to the structural geometry and connection details, the load level itself has a major influence on the fatigue life of the structure. In this study, the 13 t and 25 t load levels were compared, demonstrating a substantial difference in fatigue performance. However, even smaller variations in load can lead to significant changes in fatigue life. It should be noted that during the design phase of the test rig, it is difficult to predict all potential future measurement configurations and their corresponding load levels. For the intended use of the rig, the justified operating load is closer to a 13 t wheel load rather than 25 t, considering the rough estimation of possible cycles. The case study also identified critical locations that should be monitored more closely, thus providing valuable insight

Since the load levels in future testing of the rig are currently uncertain, an important direction for future work is to monitor the actual test load history and evaluate the cumulative fatigue damage based on the measured loading rather than relying on simplified assumed load cycles. Another key task will be to record the loads under the actual wheel-rail interaction test and their impact on the fatigue of the welds in the test frame.

References

[1] X. Yu, J. F. Aceituno, E. Kurvinen, M. K. Matikainen, P. Korkealaakso, A. Rouvinen, D. Jiang, J. L. Escalona, A. Mikkola, "Comparison of numerical and computational aspects between two constraint-based contact methods in the description of wheel/rail contacts," Multibody System Dynamics, 54(3), 303-344, 2022.

[2] J. C. O. Nielsen, R. Lundén, A. Johansson, and T. Vernersson, "Train-Track Interaction and Mechanisms of Irregular Wear on Wheel and Rail Surfaces," Vehicle System Dynamics, 40(1–3), 3–54, 2003.

[3] R. Stock, D. T. Eadie, D. Elvidge, and K. Oldknow, "Influencing rolling contact fatigue through top of rail friction modifier application – A full scale wheel–rail test rig study," Wear, 271(1–2), 134–142, 2011.

[4] S. Shrestha, M. Spiryagin, E. Bernal, Q. Wu, and C. Cole, "Recent advances in wheel-rail RCF and wear testing," Friction, 11(12), 2181–2203, 2023.

[5] R. C. Rocha, H. Ewald, A. B. Rezende, S. T. Fonseca, and P. R. Mei, "Using twin disc for applications in the railway: A systematic review," Journal of the Brazilian Society of Mechanical Sciences and Engineering, 45(4), 2023.

[6] R. Stock and R. Pippan, "RCF and wear in theory and practice—The influence of rail grade on wear and RCF," Wear, 271(1–2), 125–133, 2011.

[7] M. Naeimi, Z. Li, R. H. Petrov, J. Sietsma, and R. Dollevoet, "Development of a new downscale setup for wheel–rail contact experiments under impact loading conditions," Experimental Techniques, 42(1), 1–17, 2018.

[8] W. Zhang, J. Chen, X. Wu, and X. Jin, "Wheel/rail adhesion and analysis by using full scale roller rig," Wear, 253(1–2), 82–88, 2002.

[9] B. Jonsson, G. Dobmann, A. F. Hobbacher, M. Kassner, and G. Marquis, *IIW Guidelines on Weld Quality in Relationship to Fatigue Strength*, IIW Collection. Cham, Switzerland: Springer International Publishing, 2016, doi: 10.1007/978-3-319-19198-0.

[10] Wheel-Rail Lab: https://www.tuni.fi/en/research/full-scale-wheel-rail-lab

[11] Eurocode 3: Design of steel structures – Part 1-1: General rules and rules for buildings, SFS-EN 1993-1-1, European Committee for Standardization, 2005.

[12] Eurocode 3: Design of steel structures – Part 1-9: Fatigue,SFS-EN 1993-1-9:2025: European Committee for Standardization, 2025.

[13] A. Hobbacher, Fatigue Design of Welded Joints and Components. Cambridge, U.K.: Woodhead Publishing Ltd., 1996.

[14] W. Fricke, "IIW guideline for the assessment of weld root fatigue," Welding in the World, 57(6), 753–791, 2013.

[15] A. Ahola, H. R. Raftar, T. Björk, and O. Kukkonen, "On the interaction of axial and bending loads in the weld root fatigue strength assessment of load-carrying cruciform joints," *Welding in the World*, vol. 66, no. 4, pp. 731–744, Apr. 2022, doi: 10.1007/s40194-021-01237-6.